Electronic Supplementary Material (ESI) for Nanoscale Advances.

Electronic Supporting Information (ESI) for:

Unlocking the decoding of unknown magnetic nanobarcode signatures

By:

Mohammad Reza Zamani Kouhpanji[1,2] and Bethanie J H Stadler[1,3,*]

[1]Department of Electrical and Computer Engineering, [2]Department of Biomedical Engineering, [3]Department of Chemical Engineering and Materials Science, University of Minnesota Twin Cities, Minneapolis, MN 55455 USA.
* Corresponding author, Email: stadler [at] umn [dot] edu; Tel.: +1(612) 626-1628

Comparison between the BRM, IRM, and DCD

The standard remanence measurements are isothermal remanence magnetization (IRM) and DC demagnetization (DCD) measurements. In the IRM measurements, the MNWs must be demagnetized first (point 1 in Figure ESI-1b). An ascending field is then repeatedly applied (point 2 in Figure 1b) and removed to measure the remanence magnetization (point 3 in Figure ESI-1b). On the other hand, the DCD starts from saturation (point 1 in Figure ESI-1c) and then a descending field is repeatedly applied (point 2 in Figure ESI-1c), and removed to measure the remanence magnetization (point 3 in Figure ESI-1c). According to the Stoner-Wohlfarth model, the IRM and DCD are identical for the non-interacting MNWs. While they fall apart when the interaction fields are not negligible. Since the interaction fields dictate the initial and final magnetization states, it implies the initial magnetization state of an array of MNWs plays an important role in their magnetic remanence. Therefore, to achieve reliable and reproducible decoding, we propose a modified remanence measurement that is slightly different from the standard remanence measurements, IRM and DCD. This method, named “backward remanence magnetization (BRM)”, measures the zero-field magnetization state of the MNWs after implementing a perturbation in their initial magnetization state. Practically, the BRM measurements start by (say) positive saturation of the MNWs (point 1 in Figure

ESI-1a). The field is then reduced to a backward field (H) (point 2 in Figure ESI-1a) and then it is removed to measure the magnetization (point 3 in Figure ESI-1a). All data points are collected in the same manner, in which the MNWs are first saturated and then their initial magnetization is predefined by the H before measuring the remanence.

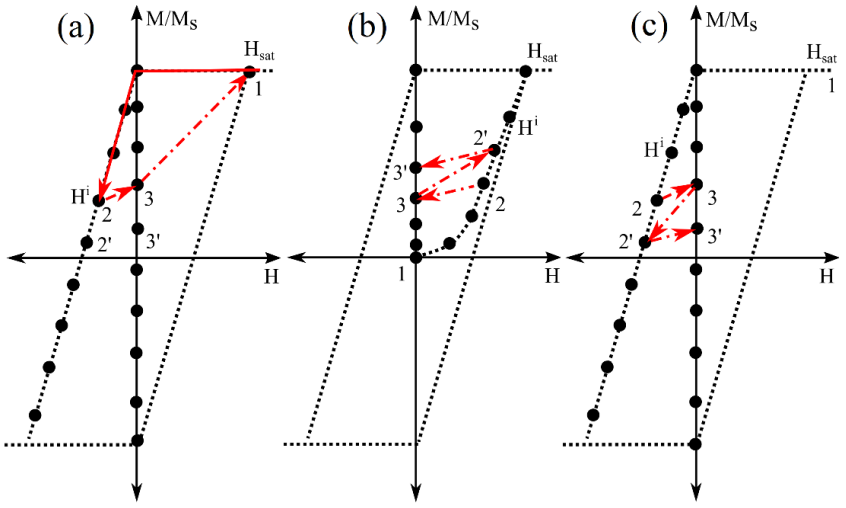

Figure ESI-1: schematically demonstrating the difference between the three remanence measurements, (a) backward remanence magnetization (BRM), (b) isothermal remanence magnetization (IRM), and (c) DC demagnetization (DCD).

Figure ESI-2 provides the BRM, IRM, and DCD data, details about the MNWs are given in the experiment section. For MNWs with negligible interaction fields ((a) and (e)), all these remanence measurements give the same results. While, they differ as the interaction fields increase (from (b) to (d) or from (f) to (h)). In most cases, the BRM data is lying between the IRM and DCD curves but closer to the DCD curves. As mentioned, each point on the standard IRM and DCD curves is not solely a function of the ascending/descending fields but also a function of the previous remanence state. In contrast, since the BRM measures the remanence of the MNWs in a systematical manner, measuring the remanence for each field started from an identical state (saturation state), it controls the number of switched MNWs much restrictively. Indeed,

the difference between the DCD and BRM determines the effects of the previous remanence state on the next remanence state. Therefore, since the magnetization direction after applying/removal of each field is completely random and stochastic in the IRM and DCD measurements, the BRM must result in a more reliable and reproducible picture of the MNWs remanence—more appealing for decoding applications.

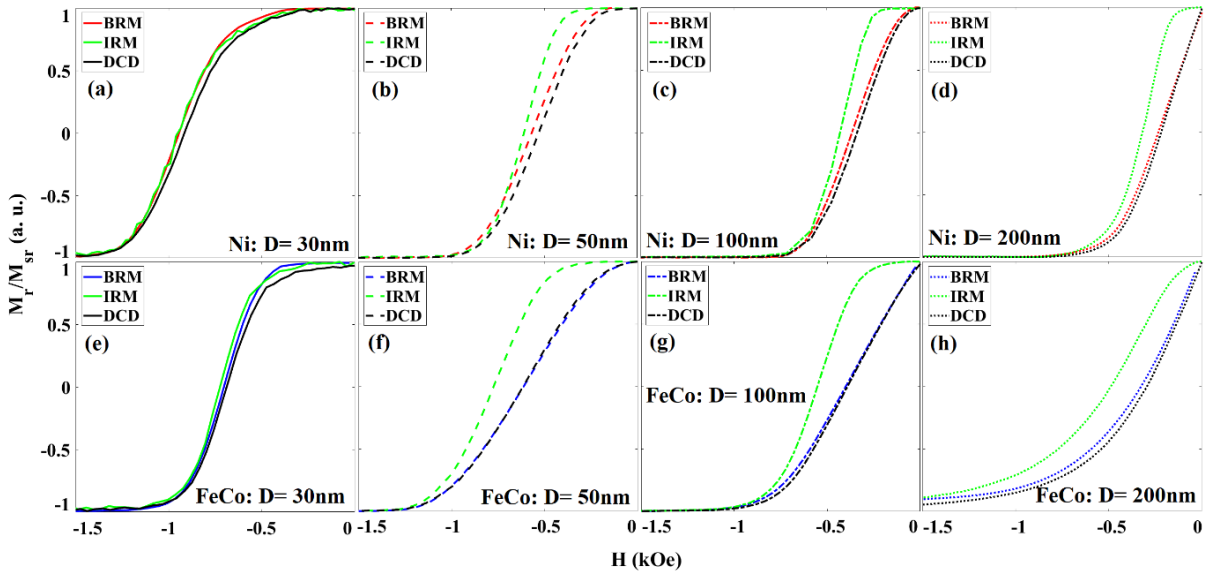

Figure ESI-2: Comparing the remanence data using the backward remanence magnetization (BRM), isothermal remanence magnetization (IRM), and DC demagnetization remanence (DCD). The top row shows the data for nickel (Ni) MNWs and the bottom row shows the data for iron cobalt (FeCo) MNWs.

Magnetic nanowires (MNWs) fabrication

All Magnetic were electrodeposited into track-etched polycarbonate (TEPC) templates with a broad range of diameters at room temperature. Prior to electrodeposition, a contact layer was made at one side of the TEPC templates to provide the electrical conductivity. The contact layer was ~10nm Ti as the adhesion layer followed by a ~300nm Au layer as the conductive layer. The electrolyte for electrodeposition of iron FeCo consisted of 0.4M boric acid, 1mM malonic acid, 0.3M ammonium chloride, 0.3mM sodium dodecyl sulfate, 6mM ascorbic acid, 0.2M iron sulfate, and 0.1M cobalt sulfate at pH ~3. The concentration ratio of the iron sulfate to cobalt sulfate was

chosen 1:2 in order to achieve the Co to Fe atomic ratio of 1:2, $Fe_{67}Co_{33}$, which is known to have the highest saturation magnetization. The electrolyte for electrodeposition of Ni was composed of 1M nickel sulfate and 0.5M boric acid at pH ~3. The electrodeposition was carried out using a three-electrode apparatus, where the cathode was the TEPC template (working electrode), the anode was a platinum mesh, and the reference electrode was a standard AgCl/Ag electrode. An alternating potential was applied for the uniform growth of the Magnetic.

SEI Images of the MNWs and the templates

D= ~30nm

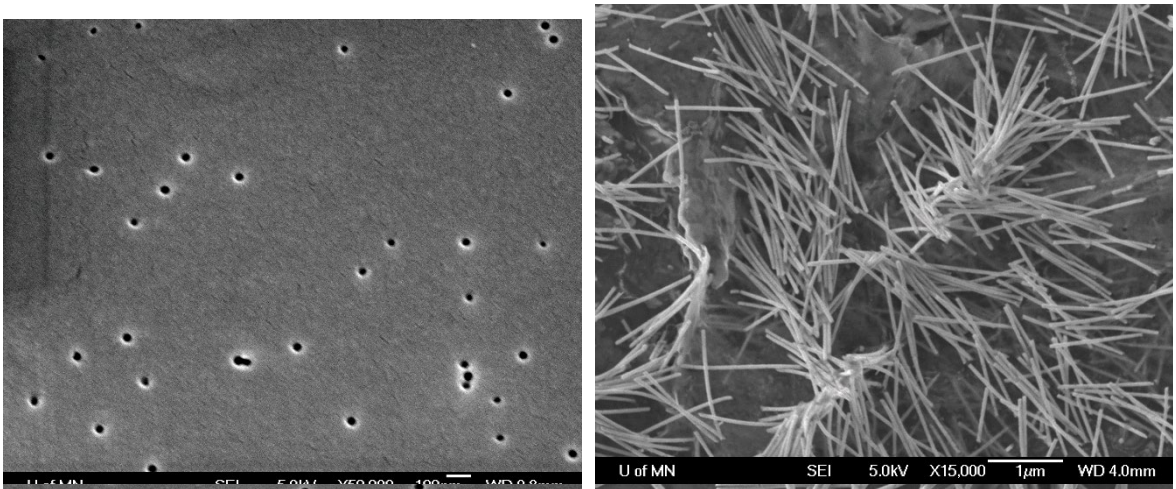

D= ~50nm

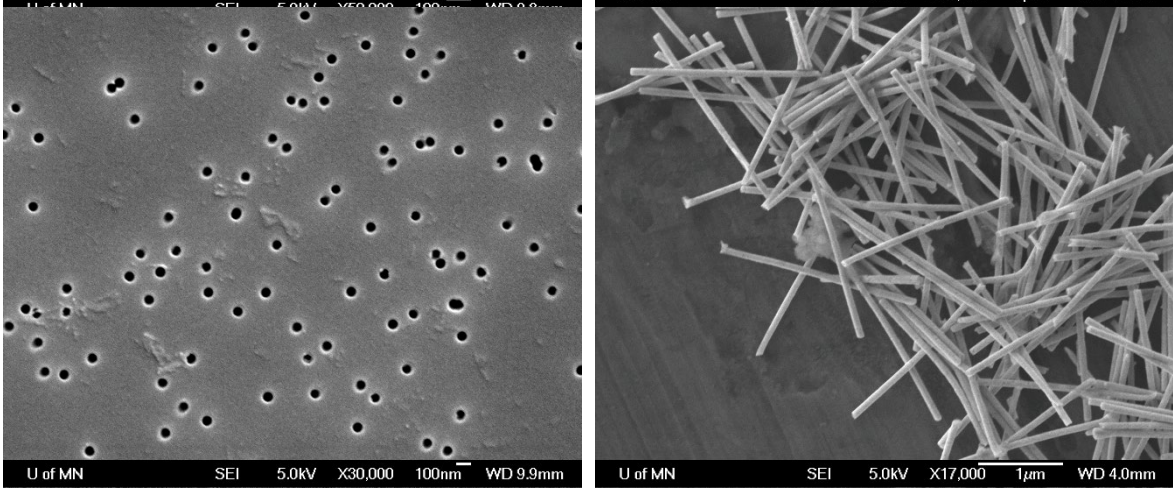

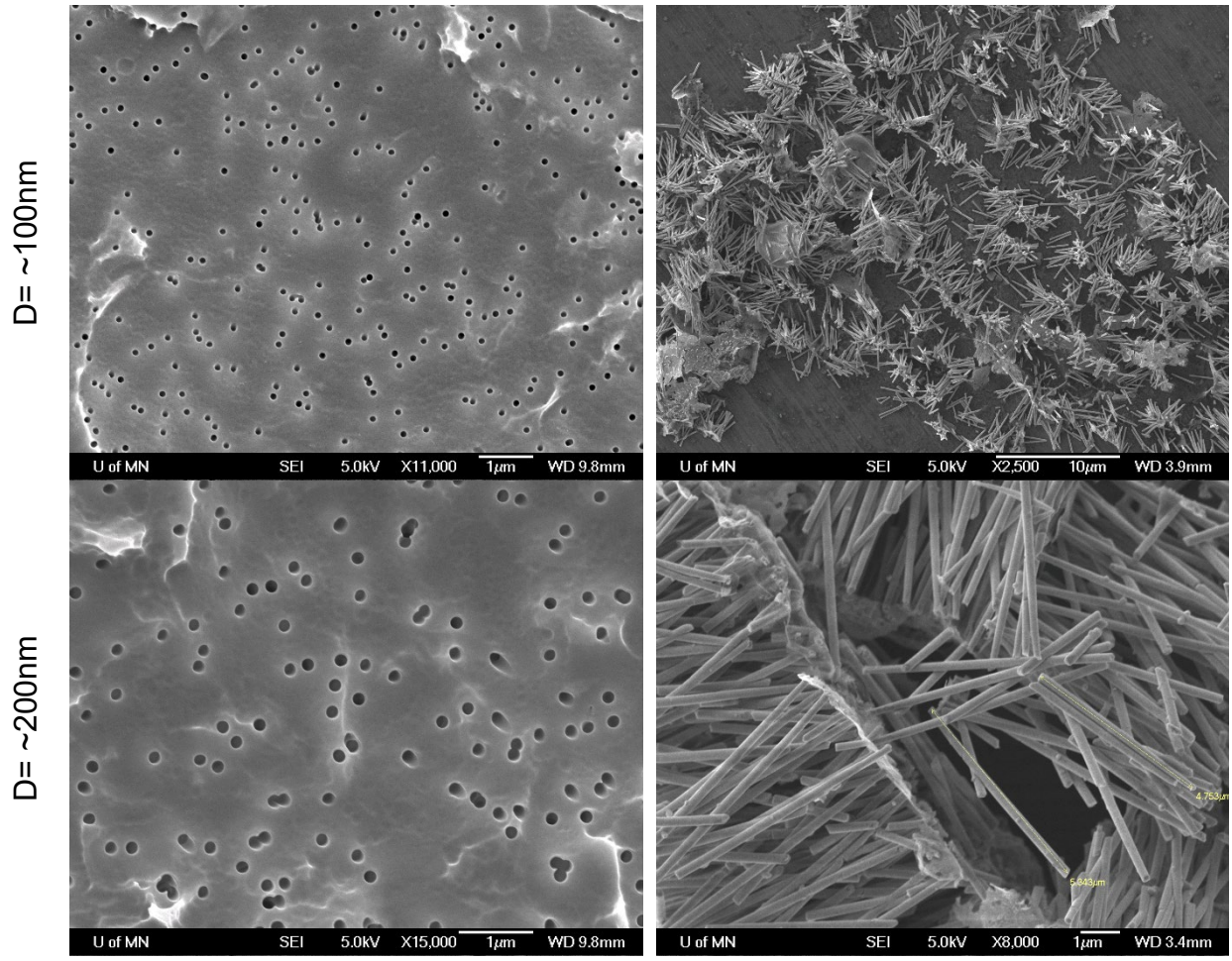

Figure ESI-3: The SEM images of the MNWs and their templates.

XRD data of the MNWs

Figure ESI-4 shows the XRD data of MNWs. The XRD data confirms the single crystal cubic structures for both Ni and FeCo MNWs. For Ni MNWs, the (111) peak is the dominant that is known to be the easy axis of the Ni crystal. Furthermore, the FeCo XRD data indicates the (100) peak to be the dominant that is known to be the easy axis for Fe FCC crystal.

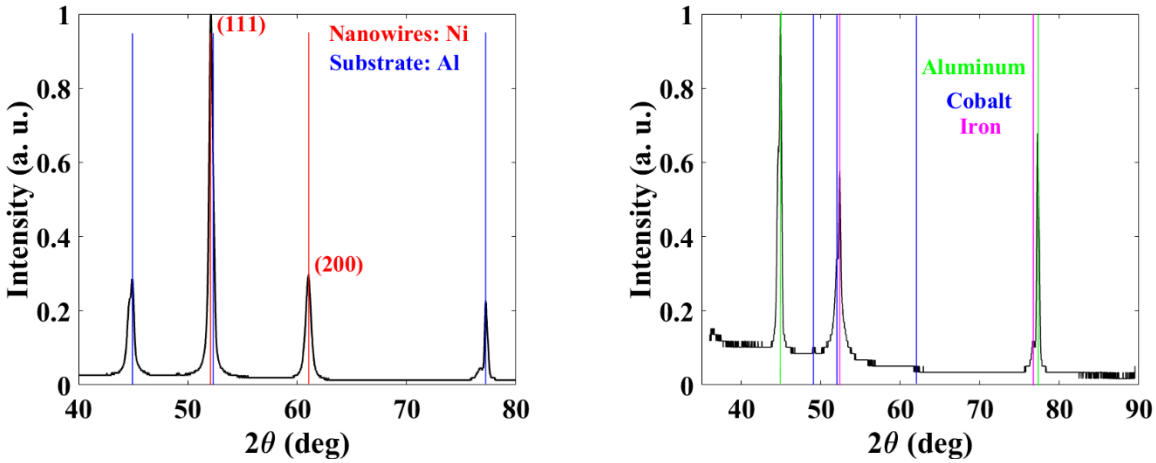

Figure ESI-4: The XRD data of the MNWs.

Protocol for the backward remanence magnetization (BRM) method:

Figure ESI-5 schematically show the data collection in the BRM method. The red arrows show the data collection for the i^{th} backward field (H_b^i) and the blue arrows show the data collection for the $(i+1)^{th}$ backward field (H_b^{i+1}). Experimentally, the measurements start from saturation of the MNWs (point 1 in Figure ESI-5) along (say) the red solid arrow. The field then is reduced to the H_b^i to set the initial magnetization state (point 2 in Figure ESI-5). Then the field is removed to measure the remanence magnetization at the zero-field (point 3 in Figure ESI-5). Before collecting the next data point, the field must return back to the saturation field (point 1 in Figure ESI-5) along (say) the red dashed line. The second data point is collected via the same procedure starting from the saturation (point 1 in Figure ESI-5) along the blue arrows.

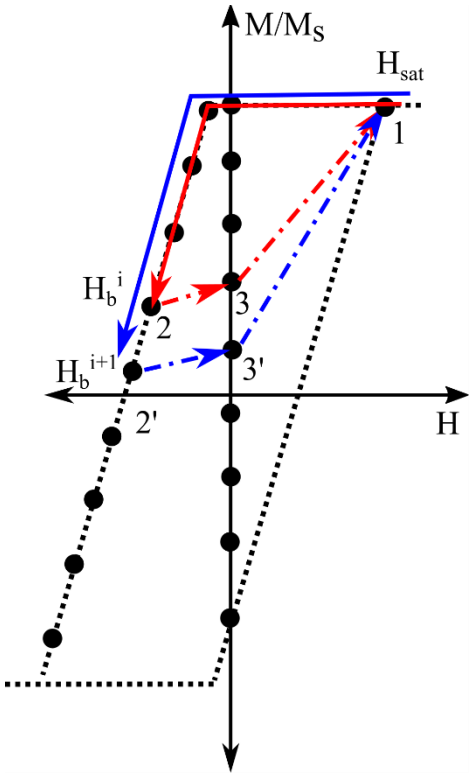

Figure ESI-5: A schematic of the BRM protocol.

Figure ESI-6 gives the raw data collected using the BRM method.

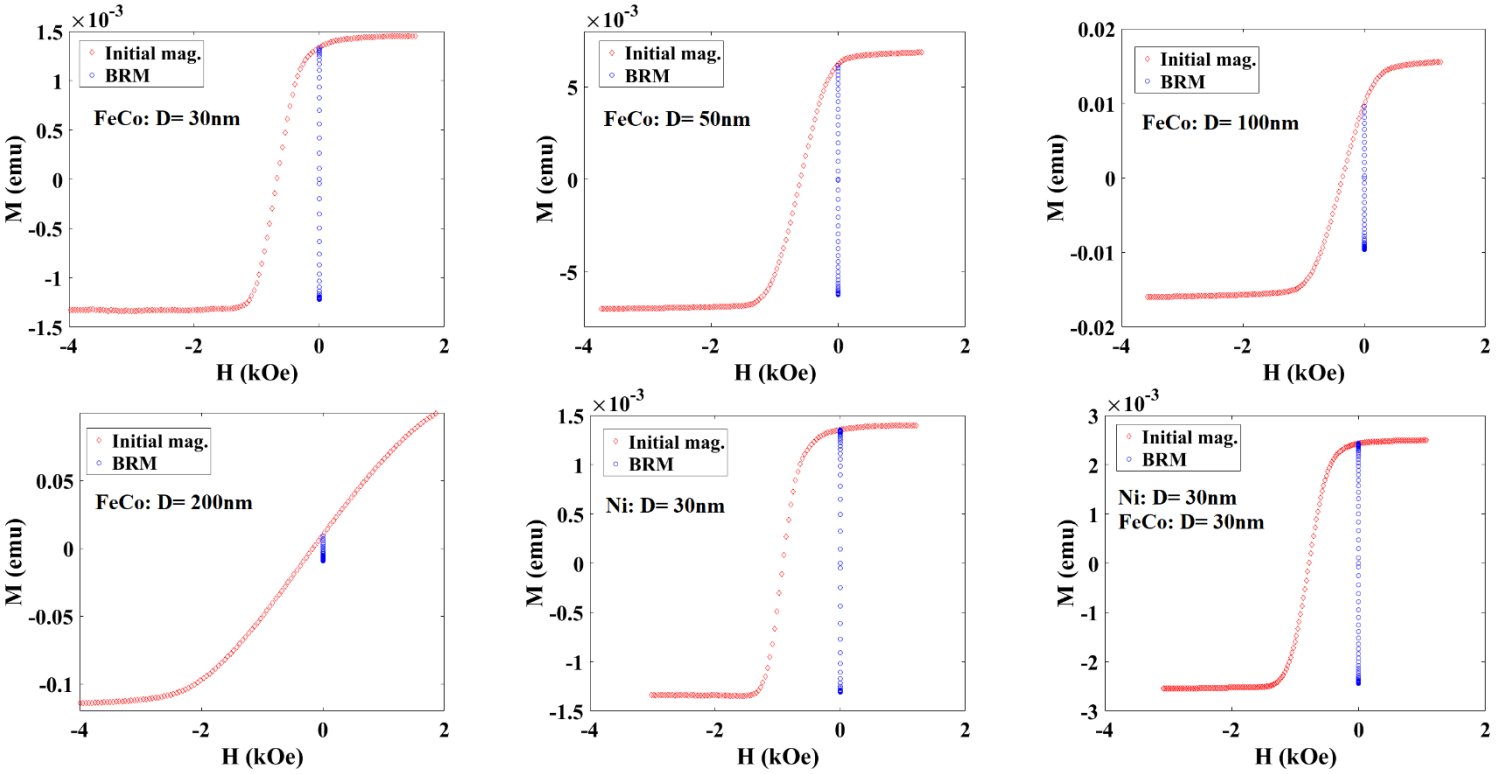

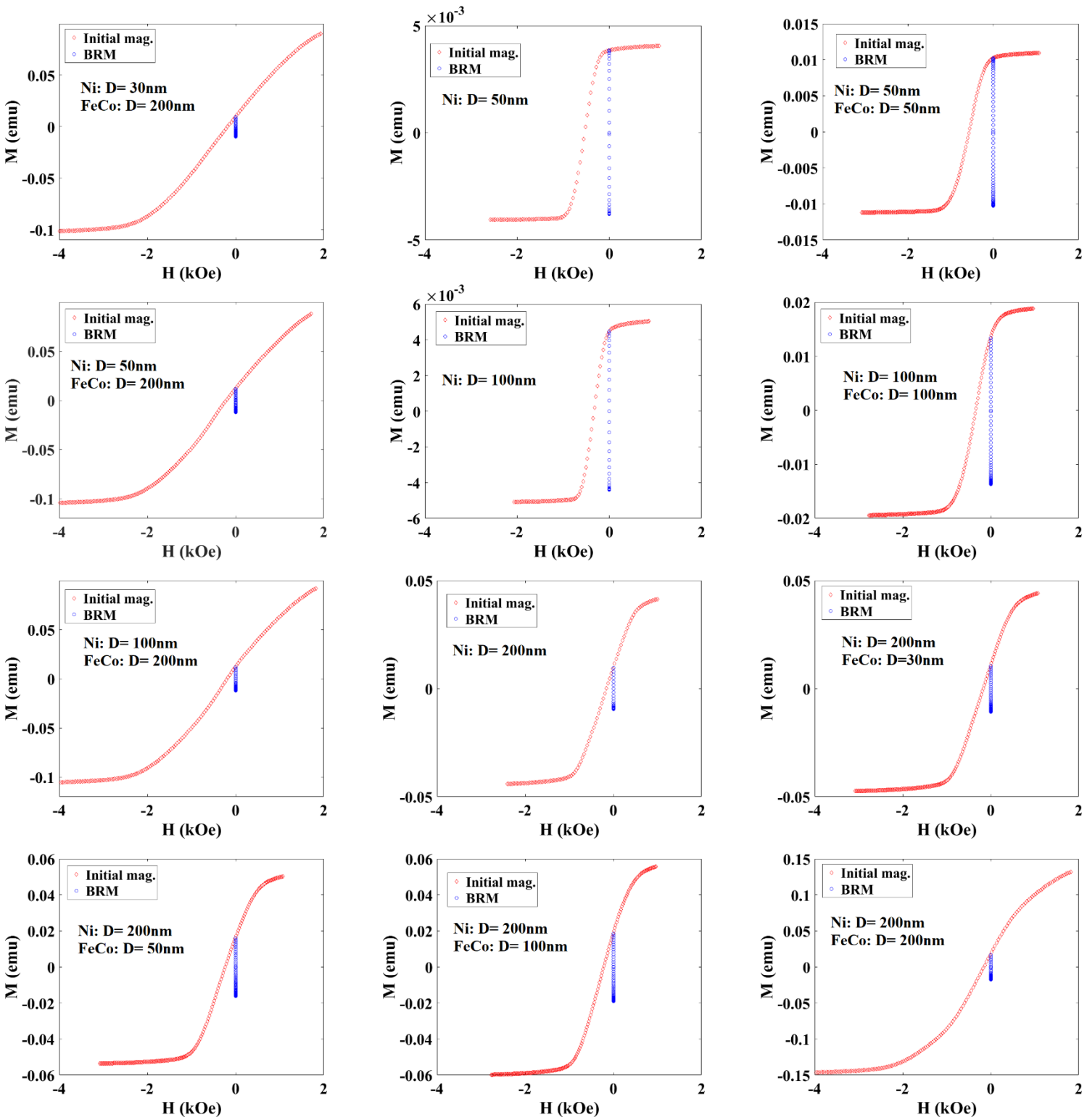

Figure ESI-6: The raw data collected using the BRM method. The red dots are basically the upper branch of the hysteresis loop, where the initial magnetization state is settled down. The blue dots are the backward remanence.

Normalized BRM data

Figures ESI-7 and ESI-8 show the normalized BRM and dBRM data of the individual MNWs and their combinations. As can be seen, the BRM (dBRM) spectra of the combination is a linear superposition of the BRM (dBRM) spectra of the individual MNWs in the combinations.

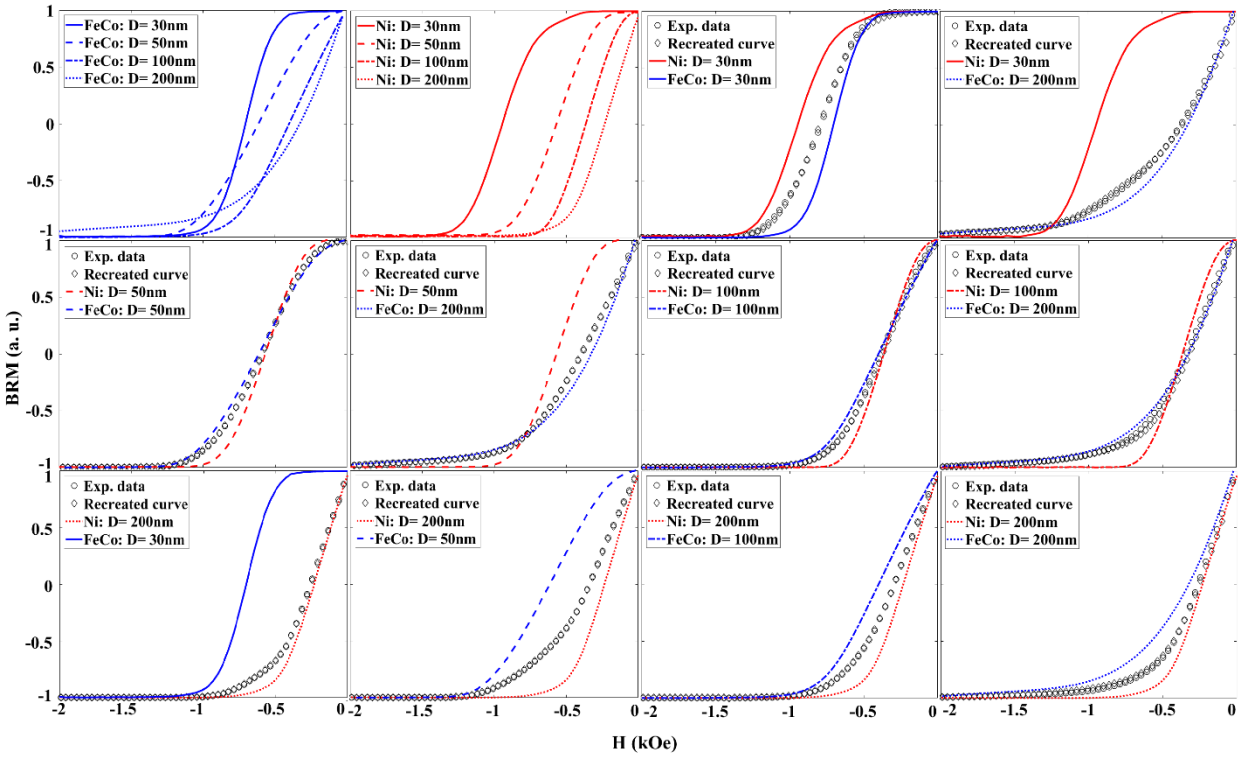

Figure ESI-7: comparing the BRM spectra of the combination and their constitute magnetic nanobarcodes as indicated in the legends.

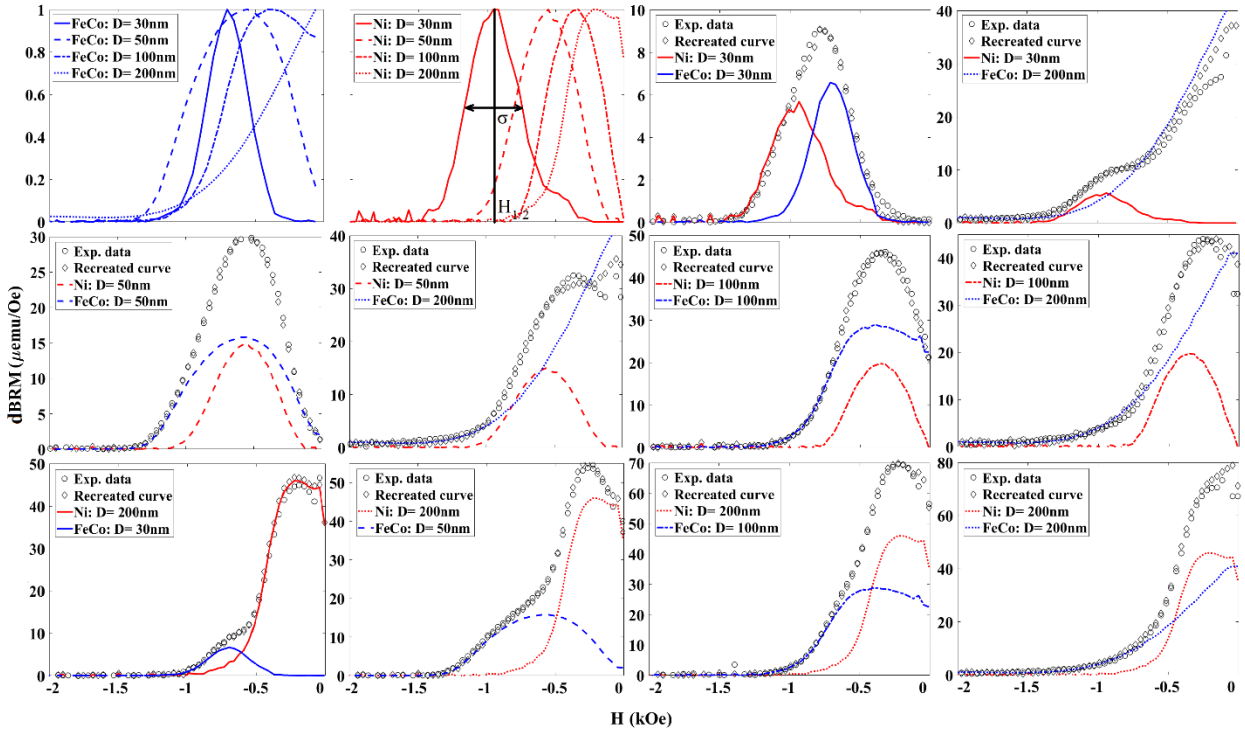

Figure ESI-8: comparing the dBRM spectra of the combination and their constitute magnetic nanobarcodes as indicated in the legends.

To find the volume ratio of each MNWs type in this combination, we wrote the "recreated curve" as follows (for example, let's consider BRM for Ni and FeCo with diameters of 50nm)

$$Recreated\ curve\ for\ BRM = \alpha_{Ni:\,D=50nm} BRM_{Ni:\,D=50nm} + \alpha_{FeCo:\,D=50nm} BRM_{FeCo:\,D=50nm} \quad (1)$$

where, α coefficients are the weight for each type. The RMS error is defined as

$$RMS = \sqrt{\frac{1}{N}\sum_{i=1}^{N}(Exp.data - Recreated\ curve)^2} \quad (2)$$

where, *N* is the number of data-points for the corresponding characteristic. The α coefficients are found while minimizing the RMS. Then, the volume ratio for *j* is calculated as follows

$$\chi_j = \frac{\alpha_j \times Volume_j}{\sum_{i=1}^{2} \alpha_i \times Volume_i} \times 100 \ (\%) \quad (3)$$

where, Volume is the initial volume of each type that was added into the combination. According to Eq. (3), if all α are 1.0, then the fit volume ratio is similar to the known volume ratio for each type of the MNWs. The results for the volume ratios are given in Figure ESI-9. Noted, the same procedure can be expanded for combinations including several types of MNWs.

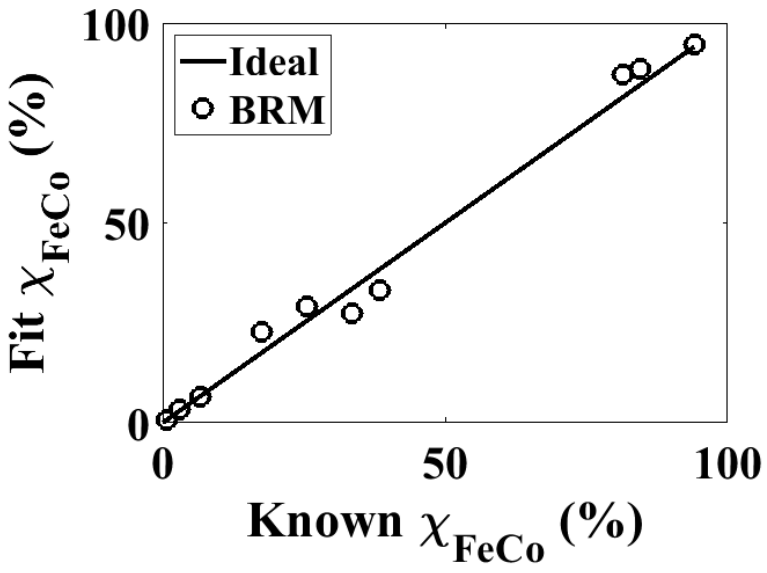

Figure ESI-9: The results for the volume ratio indicating the repeatability and stability of the magnetic moment of the MNWs.

Saturation remanence and magnetization:

Figure ESI-10 provides the saturation remanence (M_{sr}) and magnetization (M) of the MNWs.

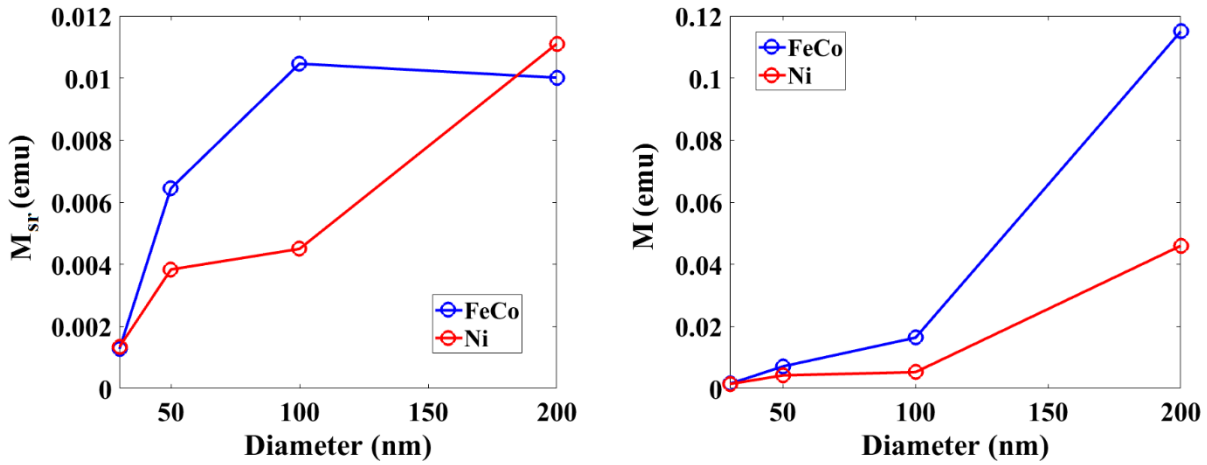

Figure ESI-10: The saturation remanence (M_{sr}) and magnetization (M) of all MNWs.